Journal of Statistics Applications & Probability
An International Journal

http://dx.doi.org/10.18576/jsap/150511

A Power Double-Transformed Sine-Lomax Distribution: Mathematical Properties, Estimation, Simulation, and Applications

Muneera A. Hussein[1], *Rana H. Khashab*[2,*], *Mundher A. Khaleel*[1], *Said G. Nassr*[3], *Ghareeb A. Marei*[4] *and Mohammed Elgarhy*[4,5]

[1]Mathematics Departments, College of Computer Science and Mathematics, Tikrit University, Iraq
[2]Mathematics Department, Faculty of Sciences, Umm Al-Qura University, Makkah, Saudi Arabia
[3]Department of Statistics and Insurance, Faculty of Commerce, Arish University, El-Arish 45511, Egypt
[4]Faculty of Computers and Information Systems, Egyptian Chinese University, Nasr City, Egypt
[5]Department of Computer Engineering, Biruni University, 34010, Istanbul, Turkey

Received: 10 Jun. 2026, Revised: 12 Aug. 2026, Accepted: 20 Aug. 2026
Published online: 1 Sep 2026

Abstract: In this paper, we develop a new four-parameter continuous lifetime model, the Power Double-Transformed Sine-Lomax (PDT-SinL) distribution. We develop this model by inserting the Lomax distribution into the Power Double-Transformed Sine-G generator. This model combines the heavy-tailed structure and simple reliability interpretation of the Lomax baseline and two additional parameters in the generator which control the transformation of the cumulative probability scale. The resulting distribution can be defined on the positive real line and can also be used to control the skewness, concentration, tail decay, survival behavior, hazard rate, and shape of the hazard rate function. We define closed-form expressions and we consider cumulative distribution function, probability density function, survival function, hazard rate, cumulative hazard rate, reversed hazard rate, and quantile function. The quantile function is expressed in the main branch of the Lambert W function which allows for the creation of random numbers. Mathematical properties are developed in detail such as validity, limiting behavior, tail asymptotics, existence of moments, integral representation of raw moments, transform behavior, entropy measures, and order statistics. Eight estimation procedures are developed for the unknown parameters: maximum likelihood, least squares, weighted least squares, Cramér-von Mises, Anderson-Darling, maximum product of spacings, percentile, and quasi-linear least squares. A Monte Carlo simulation section and a real-data application section are prepared in the same framework so that the previously obtained numerical results can be inserted directly. The proposed model therefore provides a unified heavy-tailed lifetime framework for reliability, survival, actuarial, engineering, environmental, and other positive-data applications.

Keywords: Power Double-Transformed Sine-G family; PDT-SinL distribution; Lomax distribution; heavy-tailed lifetime model; reliability analysis; Lambert *W* function; parameter estimation; Monte Carlo simulation

1 Introduction

Generated families of probability distributions have become an important part of modern distribution theory because they offer a way to enrich a simple baseline model without giving up on the basic probabilistic perspective of probability distributions. In reliability, survival analysis, engineering, actuarial science, environmental studies, and lifetime data analysis, the values often are positive and can exhibit skewness, strong kurtosis, long right tails, fast or delayed accumulation of failure probability, and hazard rate behavior that cannot be captured by a traditional two-parameter model. A generated distribution addresses this problem by applying a mathematically valid transformation to a baseline cumulative distribution function and adding additional shape parameters to the model that modify the body and tail.

Trigonometric generators are a particularly active branch of generated distribution research. Souza et al. [47] introduced the Sin-G class and showed that a sine transformation can produce flexible probability models but still have

* Corresponding author e-mail: rhkhashab@uqu.edu.sa

© 2026 NSP
Natural Sciences Publishing Cor.

the basic requirement of a valid cumulative distribution function. A cosine-based construction was also studied by Souza et al. [48], while Mahmood et al. [24] introduced a new sine-G family with some interesting mathematical properties and applications. The literature is rapidly expanding with the sine Kumaraswamy-G family [15], the sine Topp-Leone-G family [4], and the Tan-G family [49]. These were the first examples that showed that trigonometric transformations can change skewness, peakedness, and tail behavior, and they are useful when standard distributions are not very accurate.

The same research direction was carried out by other angular and trigonometric mechanisms. Alkhairy et al. [11] proposed the Arctan-X family and studied its utility in actuarial applications. Sakthivel and Rajkumar [31] studied a transmuted sine-G construction, and Souza et al. [50] introduced the Sec-G class. Mahmood et al. [25] proposed an extended cosine generalized family for reliability modeling. Hussam et al. [19] proposed a tangent exponential-G family for medical and engineering data and later suggested the sine π-power odd-G family [26], odd inverse power generalized Weibull-G [33], new sine family [34], Topp-Leone odd Fréchet-G [35], exponentiated power generalized Weibull power series family [36], power Lindley-G family [37], unit exponentiated half logistic power series class of distributions [38], new Topp-Leone Kumaraswamy Marshall-Olkin-G [39], complementary geometric Topp-Leone-G family [40], inverse Weibull-G [41], arctangent Zubair-G [42], and the sine alpha power-G family [9]. In all, the results of these studies provide a very clear methodological approach: A well-designed trigonometric generator can greatly expand the shape flexibility of a well-known baseline distribution. For more details see [43–45]

In parallel to these developments, the Lomax distribution has been an important model for positive and heavy-tailed observations. The survival function has a simple Pareto-type structure, and hyperbolically the hazard rate decreases. Such features make it attractive in reliability, income and insurance modeling, waiting-time studies, network and engineering applications, and many other situations where large observations are more frequent than exponentially tailed models predict. Nawaf et al. [27] studied a hybrid odd Lomax-Fréchet construction, Algarni et al. [8] developed a truncated inverse Lomax generated family for biomedical data, and Noori and Khaleel [28] considered a Gompertz-neutrosophic Lomax extension. The contributions of these papers show that the Lomax baseline can be used as a useful building block for more flexible models. Related recent lifetime models include extended Lindley-type and one-parameter decreasing-hazard distributions [20, 29] and an odds-based Weibull model for engineering failure-time data [3].

The inferential side of generated distributions is equally important. A flexible model can be useful only if it can be estimated reliably and the numerical behavior can be checked by repeated sampling. The present framework consists of a broad estimation approach. Besides maximum likelihood, it takes into account least squares and weighted least squares, which are closely related to classical reliability estimation ideas [13, 22]. It also considers Cramér-von Mises estimation [16], Anderson-Darling estimation [12], maximum product of spacings [46], percentile estimation [51], and a quasi-linear transformation approach related to the general principle of quasi-linear estimation [17]. The recent work in the same field on distributional problems also shows the importance of comparing different inferential approaches to the problem instead of using a single estimator [10, 21]. Classical and Bayesian procedures for censored lifetime data, including Markov chain Monte Carlo and Tierney–Kadane approximations, have been developed in [5, 7], and stress-strength reliability inference under censored and record data has been studied in [2, 6, 18, 30]. Applied validation is also an important part of the distribution development. Flexible positive data models were tested in technological adoption data [23], component failure data [32], and many other settings. This shows that a proposed model should not only be evaluated on theoretical grounds but also on the basis of information criteria, goodness-of-fit statistics, graphical diagnostics and numerical stability. A good model should provide a good balance between fit quality and complexity and should be computationally stable compared with other existing models.

We follow the general structure of the Power Double-Transformed Sine-G model, but we use the Lomax distribution as the baseline model. The motivation is obvious. The Lomax model has a good heavy-tailed reliability structure, but it is not able to control the specifics of the density shape and the accumulation of the probability as a classical two-parameter model. We add more positive parameters to the Power Double-Transformed Sine model. These parameters first change the baseline probability by a double transformation and then pass the result through a sine-power map. This results in a four-parameter model with positive support but more control of the distributional shape. The major methodological gap in the reference we are working on is that we have not systematically developed the Power Double-Transformed Sine-Lomax specialization and its reliability functions, closed-form quantile, tail structure, moment conditions, entropy measures, order statistics, etc. in a systematic way, and a complete eight-method estimation framework.

In this work, we fill this gap. First we provide the PDT-SinL distribution as derived from the Lomax baseline, then we show its main reliability function and its mathematical properties. Third we obtain the order of the upper tail. Fourth, a Lambert-W quantile representation is presented in order to make simulation simple. Finally, we present eight estimation methods in a consistent notation. We provide sections for Monte Carlo and real data analysis that have already been carried out separately.The rest of the paper is organized as follows. Section 2 presents the general Power Double-Transformed Sine-G generator. In Section 3, we develop the PDT-SinL distribution and define its distribution and reliability functions. In Section 4, we develop some of its most important mathematical properties. In Section 5, we define eight parameter estimation procedures. In Section 6, we provide the simulation framework and reserved positions for the numerical results

© 2026 NSP
Natural Sciences Publishing Cor.

that were completed. In Section 7, we provide the real data application framework. The last section summarizes the main theoretical and practical results.

2 General Power Double-Transformed Sine-G Generator

Let $G(x;\eta)$ be a baseline cumulative distribution function with density $g(x;\eta)$, where η denotes the baseline parameter vector. Define the double-transformed probability function

$$T(x) = G(x)\exp\{1-G(x)\}, \qquad 0 \le T(x) \le 1. \tag{1}$$

Because $0 \le G(x) \le 1$, the function $T(x)$ maps the baseline probability scale into $[0,1]$. Its derivative is

$$T'(x) = g(x)\exp\{1-G(x)\}\{1-G(x)\}. \tag{2}$$

For generator parameters $\delta > 0$ and $\theta > 0$, define

$$Z(x) = \frac{\pi}{2}\left[T(x)\right]^{\delta}. \tag{3}$$

The cumulative distribution function of the general Power Double-Transformed Sine-G family is

$$F(x) = \left[\sin Z(x)\right]^{\theta} = \left[\sin\left\{\frac{\pi}{2}\left(G(x)e^{1-G(x)}\right)^{\delta}\right\}\right]^{\theta}. \tag{4}$$

Differentiating (4) gives the general density

$$f(x) = \frac{\pi\delta\theta}{2}g(x)\{1-G(x)\}e^{1-G(x)}\left[T(x)\right]^{\delta-1} \times \left[\sin Z(x)\right]^{\theta-1}\cos Z(x) \tag{5}$$

The survival function is

$$\overline{F}(x) = 1 - F(x) = 1 - \left[\sin Z(x)\right]^{\theta}. \tag{6}$$

The hazard-rate function is

$$h(x) = \frac{f(x)}{1-\left[\sin Z(x)\right]^{\theta}}. \tag{7}$$

The cumulative hazard function is

$$H(x) = -\log\left\{1-\left[\sin Z(x)\right]^{\theta}\right\}, \tag{8}$$

and the reversed hazard-rate function is

$$r(x) = \frac{f(x)}{\left[\sin Z(x)\right]^{\theta}}. \tag{9}$$

These expressions are valid for every absolutely continuous baseline distribution for which G and g are well defined.

3 Power Double-Transformed Sine-Lomax Distribution

Let X follow a Lomax distribution with scale parameter $\alpha > 0$ and shape parameter $\lambda > 0$. Its cumulative distribution function and probability density function are

$$G(x;\alpha,\lambda) = 1 - \left(1+\frac{x}{\alpha}\right)^{-\lambda}, \qquad x > 0, \tag{10}$$

and

$$g(x;\alpha,\lambda) = \frac{\lambda}{\alpha}\left(1+\frac{x}{\alpha}\right)^{-(\lambda+1)}, \qquad x > 0. \tag{11}$$

© 2026 NSP
Natural Sciences Publishing Cor.

For compact notation, define

$$S(x) = \left(1 + \frac{x}{\alpha}\right)^{-\lambda}, \qquad G(x) = 1 - S(x), \tag{12}$$

so that

$$T(x) = [1 - S(x)]\, e^{S(x)}, \qquad Z(x) = \frac{\pi}{2}\,[T(x)]^{\delta}. \tag{13}$$

The four positive parameters of the proposed model are therefore

$$\psi = (\delta, \theta, \alpha, \lambda)^{\mathsf{T}}, \qquad \delta, \theta, \alpha, \lambda > 0. \tag{14}$$

Here, δ and θ are the generator parameters, α is the Lomax scale parameter, and λ is the Lomax shape parameter.

Substituting the Lomax baseline into the general generator yields the cumulative distribution function of the Power Double-Transformed Sine-Lomax (PDT-SinL) distribution:

$$F(x) = \left[\sin\left\{\frac{\pi}{2}\left([1 - S(x)]\, e^{S(x)}\right)^{\delta}\right\}\right]^{\theta}, \qquad x > 0. \tag{15}$$

Equivalently,

$$F(x) = \left[\sin\left\{\frac{\pi}{2}\left[\left(1 - \left(1 + \frac{x}{\alpha}\right)^{-\lambda}\right)\exp\left(\left(1 + \frac{x}{\alpha}\right)^{-\lambda}\right)\right]^{\delta}\right\}\right]^{\theta}. \tag{16}$$

The boundary conditions are $F(0) = 0$ and $\lim_{x\to\infty} F(x) = 1$. Using (5), the PDT-SinL density can be expressed compactly as

$$f(x) = \frac{\pi\delta\theta\lambda}{2\alpha}\left(1 + \frac{x}{\alpha}\right)^{-(2\lambda+1)} e^{S(x)}\,[T(x)]^{\delta-1} \times [\sin Z(x)]^{\theta-1}\cos Z(x), \qquad x > 0 \tag{17}$$

Every factor in (17) is nonnegative for $x > 0$ and positive model parameters. The density integrates to one because it is the derivative of the valid CDF in (15).

The survival function is

$$\overline{F}(x) = 1 - \left[\sin\left\{\frac{\pi}{2}\left[\left(1 - \left(1 + \frac{x}{\alpha}\right)^{-\lambda}\right)\exp\left(\left(1 + \frac{x}{\alpha}\right)^{-\lambda}\right)\right]^{\delta}\right\}\right]^{\theta}. \tag{18}$$

The hazard-rate function becomes

$$h(x) = \frac{\frac{\pi\delta\theta\lambda}{2\alpha}\left(1 + \frac{x}{\alpha}\right)^{-(2\lambda+1)} e^{S(x)}\,[T(x)]^{\delta-1}\,[\sin Z(x)]^{\theta-1}\cos Z(x)}{1 - \left[\sin\left\{\frac{\pi}{2}\left[\left(1 - \left(1 + \frac{x}{\alpha}\right)^{-\lambda}\right)\exp\left(\left(1 + \frac{x}{\alpha}\right)^{-\lambda}\right)\right]^{\delta}\right\}\right]^{\theta}}. \tag{19}$$

The cumulative hazard function is

$$H(x) = -\log\left\{1 - \left[\sin\left\{\frac{\pi}{2}\left[\left(1 - \left(1 + \frac{x}{\alpha}\right)^{-\lambda}\right)\exp\left(\left(1 + \frac{x}{\alpha}\right)^{-\lambda}\right)\right]^{\delta}\right\}\right]^{\theta}\right\}, \tag{20}$$

while the reversed hazard-rate function is

$$r(x) = \frac{\frac{\pi\delta\theta\lambda}{2\alpha}\left(1 + \frac{x}{\alpha}\right)^{-(2\lambda+1)} e^{S(x)}\,[T(x)]^{\delta-1}\,[\sin Z(x)]^{\theta-1}\cos Z(x)}{\left[\sin\left\{\frac{\pi}{2}\left[\left(1 - \left(1 + \frac{x}{\alpha}\right)^{-\lambda}\right)\exp\left(\left(1 + \frac{x}{\alpha}\right)^{-\lambda}\right)\right]^{\delta}\right\}\right]^{\theta}}. \tag{21}$$

The Lomax baseline has the decreasing hazard $\lambda/(\alpha + x)$. In the proposed model, the additional sine-power transformation modifies the curvature of the hazard through δ and θ. Consequently, graphical analysis under different parameter combinations is important for identifying the practical range of hazard shapes generated by the model.

© 2026 NSP
Natural Sciences Publishing Cor.

The CDF, PDF, and survival function are plotted under several parameter combinations to study the effect of δ, θ, α, and λ. The CDF plots should verify monotone accumulation from zero to one. The PDF plots should be used to study peak location, concentration, skewness, and right-tail decay. The survival plots should show how the parameters modify persistence and failure probability across time.

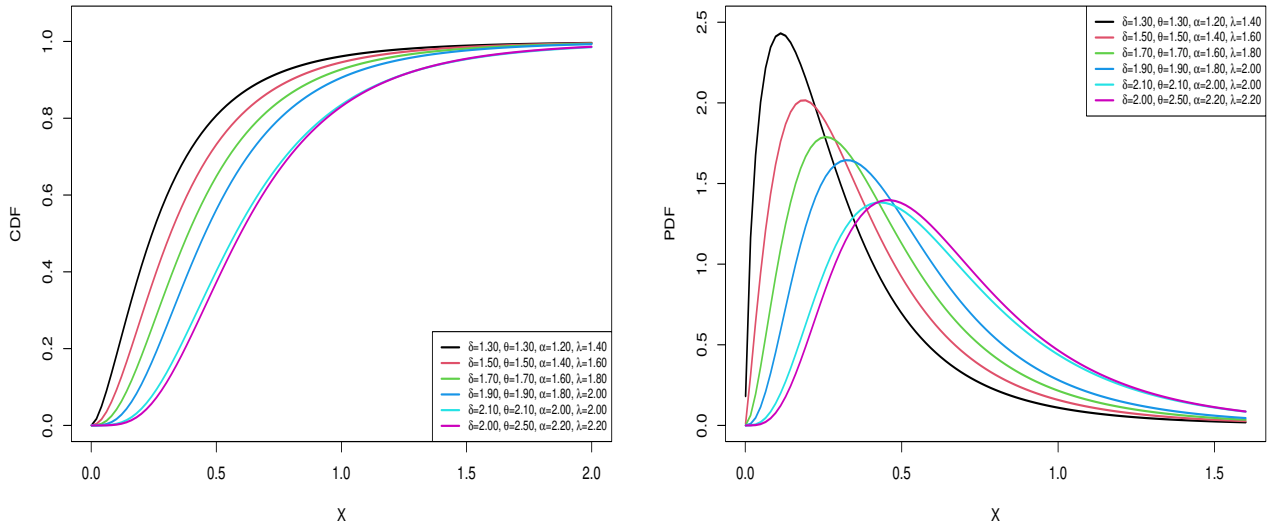


Fig. 1: CDF and pdf curves of the PDT-SinL distribution under selected parameter combinations.

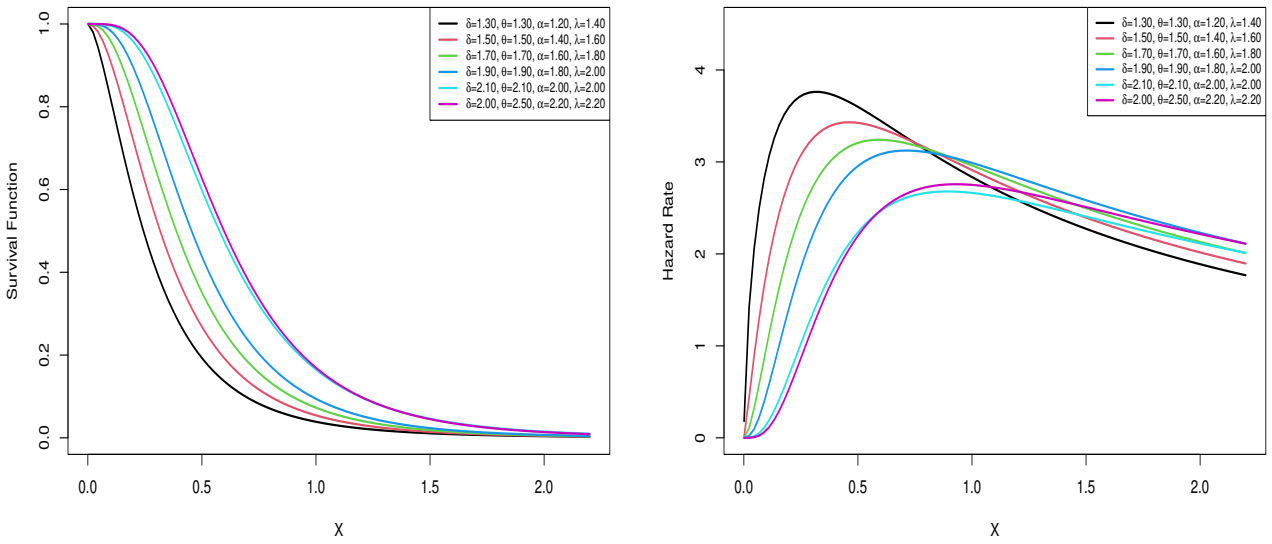


Fig. 2: Survival and hazard curves of the PDT-SinL distribution under selected parameter combinations.

4 Mathematical Properties

4.1 Validity of the distribution

For $x \geq 0$,

$$0 \leq G(x) = 1 - S(x) < 1, \qquad 0 < S(x) \leq 1. \tag{22}$$

The function $\phi(g) = ge^{1-g}$ is increasing on $0 \leq g \leq 1$ because

© 2026 NSP
Natural Sciences Publishing Cor.

$$\phi'(g) = e^{1-g}(1-g) \geq 0. \tag{23}$$

Thus $0 \leq T(x) \leq 1$. Because $\delta > 0$,

$$0 \leq [T(x)]^{\delta} \leq 1, \tag{24}$$

and therefore

$$0 \leq Z(x) = \frac{\pi}{2}[T(x)]^{\delta} \leq \frac{\pi}{2}. \tag{25}$$

The sine function is increasing and nonnegative on this interval. Raising it to the positive power θ preserves monotonicity. Hence $F(x)$ is nondecreasing. Furthermore,

$$F(0) = 0, \qquad \lim_{x\to\infty} F(x) = 1. \tag{26}$$

Consequently, (15) is a valid CDF. Since the factors in (17) are nonnegative, $f(x) \geq 0$, and the density integrates to one.

4.2 Quantile function

Let $0 < p < 1$ and set $F(x) = p$. From (15),

$$\sin Z(x) = p^{1/\theta}. \tag{27}$$

Because $0 \leq Z(x) \leq \pi/2$, the principal inverse sine gives $Z(x) = \sin^{-1}\left(p^{1/\theta}\right)$. Therefore,

$$T(x) = y_p, \qquad y_p = \left[\frac{2}{\pi}\sin^{-1}\left(p^{1/\theta}\right)\right]^{1/\delta}. \tag{28}$$

Recall that $T(x) = G(x)e^{1-G(x)}$. Let $s = 1 - G(x)$. Then $(1-s)e^s = y_p$. Write $u = s - 1$. Equation becomes

$$ue^u = -\frac{y_p}{e}. \tag{29}$$

Hence, using the principal Lambert branch W_0, $s = 1 + W_0\left(-\frac{y_p}{e}\right)$. For the Lomax baseline, $s = S(x) = (1 + x/\alpha)^{-\lambda}$. Thus

$$\left(1 + \frac{x}{\alpha}\right)^{-\lambda} = 1 + W_0\left(-\frac{y_p}{e}\right). \tag{30}$$

The PDT-SinL quantile function is therefore

$$Q(p) = \alpha\left\{\left[1 + W_0\left(-\frac{y_p}{e}\right)\right]^{-1/\lambda} - 1\right\}, \tag{31}$$

Equation (31) gives a direct and computationally efficient method for generating random observations from the proposed distribution. The median is obtained by setting $p = 1/2$ in (31):

$$Med(X) = Q(0.5). \tag{32}$$

Similarly, the first and third quartiles are $Q(0.25)$ and $Q(0.75)$. Quantile-based measures of skewness and kurtosis can therefore be computed without numerical integration. For example, Bowley skewness is

$$B = \frac{Q(0.75) + Q(0.25) - 2Q(0.50)}{Q(0.75) - Q(0.25)}, \tag{33}$$

and a Moors-type quantile kurtosis measure can be constructed from octiles. These measures are especially useful for heavy-tailed distributions because they remain stable even when high-order moments do not exist.

© 2026 NSP
Natural Sciences Publishing Cor.

4.3 Tail behavior

The Lomax baseline survival term is $S(x) = \left(1+\frac{x}{\alpha}\right)^{-\lambda}$. As $x \to \infty$, $S(x) \to 0$. A local expansion gives

$$[1-S(x)]\, e^{S(x)} = 1 - \frac{S(x)^2}{2} + O\left(S(x)^3\right). \tag{34}$$

Hence

$$[T(x)]^{\delta} = 1 - \frac{\delta}{2} S(x)^2 + O\left(S(x)^3\right), \tag{35}$$

and therefore

$$Z(x) = \frac{\pi}{2} - \frac{\pi\delta}{4} S(x)^2 + O\left(S(x)^3\right). \tag{36}$$

Using $\sin(\pi/2 - v) = cosv = 1 - v^2/2 + o\left(v^2\right)$ gives $1 - F(x) \sim \frac{\theta\pi^2\delta^2}{32} S(x)^4$. Consequently,

$$\overline{F}(x) \sim \frac{\theta\pi^2\delta^2}{32} \left(1+\frac{x}{\alpha}\right)^{-4\lambda}, \qquad x \to \infty. \tag{37}$$

Thus the proposed model remains polynomially tailed, but the effective tail exponent is 4λ. The corresponding density satisfies

$$f(x) \sim \frac{\theta\pi^2\delta^2\lambda}{8\alpha} \left(1+\frac{x}{\alpha}\right)^{-(4\lambda+1)}. \tag{38}$$

The hazard function therefore has the asymptotic form

$$h(x) \sim \frac{4\lambda}{x+\alpha}, \qquad x \to \infty. \tag{39}$$

This result is important because it gives a direct interpretation of the far-right reliability behavior of the proposed model.

4.4 Raw moments

This part provides a useful series representation of the Power Double-Transformed Sine-G family and specializes it to the PDT-SinL model. The generator parameters are $\delta > 0$ and $\theta > 0$, while $\alpha > 0$ and $\lambda > 0$ are the Lomax scale and shape parameters. Throughout,

$$G(x) = 1 - \left(1+\frac{x}{\alpha}\right)^{-\lambda}, \qquad g(x) = \frac{\lambda}{\alpha}\left(1+\frac{x}{\alpha}\right)^{-(\lambda+1)},$$

$$T(x) = G(x)e^{1-G(x)}, \qquad Z(x) = \frac{\pi}{2}\left[T(x)\right]^{\delta}.$$

The same sine-power expansion used in the useful representation of the generated family is retained inside the moment derivation. Write

$$\sin^{\theta}(z) = \sum_{k=0}^{\infty} a_k(\theta) z^{\theta+2k},$$

where the coefficients $a_k(\theta)$ are those defined by the sine-power expansion. Equivalently, for general positive θ, they are the coefficients of

$$\left(\frac{\sin z}{z}\right)^{\theta} = \sum_{k=0}^{\infty} a_k(\theta) z^{2k},$$

With $a_0(\theta) = 1, \quad a_1(\theta) = -\frac{\theta}{6}, \quad a_2(\theta) = \frac{\theta(5\theta-2)}{360}, \quad a_3(\theta) = -\frac{\theta\left(35\theta^2-42\theta+16\right)}{45360}, \ldots$

Differentiating the sine-power series gives

© 2026 NSP
Natural Sciences Publishing Cor.

$$\sin^{\theta-1}(z)\cos(z) = \frac{1}{\theta}\sum_{k=0}^{\infty} a_k(\theta)(\theta+2k)z^{\theta+2k-1}.$$

Substitution into the PDT-SinG density gives

$$f(x) = T'(x)\sum_{k=0}^{\infty} B_k\,[T(x)]^{p_k-1},$$

where

$$p_k = \delta(\theta+2k), \qquad B_k = \frac{\pi\delta}{2}a_k(\theta)(\theta+2k)\left(\frac{\pi}{2}\right)^{\theta+2k-1}.$$

Since

$$T'(x) = g(x)e^{1-G(x)}\,[1-G(x)],$$

we obtain

$$f(x) = g(x)\,[1-G(x)]\sum_{k=0}^{\infty} B_k G(x)^{p_k-1}e^{p_k[1-G(x)]}.$$

Using the same exponential-series step as in the useful representation,

$$e^{p_k[1-G(x)]} = e^{p_k}\sum_{z=0}^{\infty}\frac{(-p_k)^z}{z!}G(x)^z,$$

hence

$$f(x) = \sum_{k=0}^{\infty}\sum_{z=0}^{\infty} D_{kz}\,g(x)\,[1-G(x)]\,G(x)^{\nu_{kz}-1},$$

where

$$D_{kz} = B_k e^{p_k}\frac{(-p_k)^z}{z!}, \qquad \nu_{kz} = p_k+z.$$

This is the direct continuation of the generated-family expansion. Therefore, for an integer moment order m,

$$\mu'_m = \sum_{k=0}^{\infty}\sum_{z=0}^{\infty} D_{kz}\int_0^{\infty} x^m g(x)\,[1-G(x)]\,G(x)^{\nu_{kz}-1}\,dx.$$

With $y = G(x)$, $dy = g(x)dx$, and $x = \alpha\left[(1-y)^{-1/\lambda}-1\right]$, the inner integral becomes

$$\mathscr{M}_m(\nu) = \alpha^m\int_0^1\left[(1-y)^{-1/\lambda}-1\right]^m(1-y)y^{\nu-1}\,dy.$$

For integer m, expansion of the binomial gives, whenever term-by-term integration is absolutely valid,

$$\mathscr{M}_m(\nu) = \alpha^m\sum_{j=0}^{m}(-1)^{m-j}\binom{m}{j}B\left(\nu, 2-\frac{j}{\lambda}\right).$$

Thus the original generated-family expansion already converts the raw moments to beta-function sums. For proofs over the full moment-existence range, however, it is more efficient to regroup the same density on the Lomax survival scale. Put

$$s = S(x) = 1-G(x) = \left(1+\frac{x}{\alpha}\right)^{-\lambda}, \qquad T(s) = (1-s)e^s,$$

and define the regular coefficient function

© 2026 NSP
Natural Sciences Publishing Cor.

$$C(s)=\frac{\pi\delta\theta}{2}e^{s}\left[T(s)\right]^{\delta-1}\left[\sin\left(\frac{\pi}{2}\left[T(s)\right]^{\delta}\right)\right]^{\theta-1}\frac{\cos\left(\frac{\pi}{2}\left[T(s)\right]^{\delta}\right)}{s^{2}}=\sum_{n=0}^{\infty}c_{n}s^{n}.$$

The division by s^2 is regular because $\cos\{\frac{\pi}{2}\left[T(s)\right]^{\delta}\}=O\left(s^{2}\right)$ as $s\to 0$. Hence

$$c_{n}=\frac{1}{n!}\left.\frac{d^{n}}{ds^{n}}C(s)\right|_{s=0},$$

with the first coefficients

$$c_{0}=\frac{\theta\pi^{2}\delta^{2}}{8},\qquad c_{1}=\frac{5\theta\pi^{2}\delta^{2}}{24},\qquad c_{2}=\frac{\theta\pi^{2}\delta^{2}(26-9\delta)}{96},\qquad c_{3}=\frac{7\theta\pi^{2}\delta^{2}(22-15\delta)}{480}.$$

Since $g(x)=(\lambda/\alpha)s^{1+1/\lambda}$, the PDT-SinL density can now be written in the following tail-preserving power-series form:

$$f(x)=\frac{\lambda}{\alpha}\sum_{n=0}^{\infty}c_{n}\left(1+\frac{x}{\alpha}\right)^{-[\lambda(n+4)+1]},\qquad x>0. \tag{40}$$

This representation preserves the exact fourth-order cancellation produced by the sine-cosine mechanism. It also immediately yields the normalization identity

$$\sum_{n=0}^{\infty}\frac{c_{n}}{n+4}=1.$$

Using Equation (40), the rth raw moment is

$$\mu_{r}^{'}=E\left(X^{r}\right)=\int_{0}^{\infty}x^{r}f(x)\,dx$$

Substituting (40) yields

$$\mu_{r}^{'}=E\left(X^{r}\right)=\int_{0}^{\infty}x^{r}\frac{\lambda}{\alpha}\sum_{n=0}^{\infty}c_{n}\left(1+\frac{x}{\alpha}\right)^{-[\lambda(n+4)+1]}dx$$

$$\mu_{r}^{'}=E\left(X^{r}\right)=\lambda\alpha^{r}\sum_{n=0}^{\infty}c_{n}B\left(r+1,\lambda(n+4)-r\right),\qquad 0\le r<4\lambda. \tag{41}$$

Because the smallest tail power in Equation (40) corresponds to $n=0$, the exact existence condition is

$$E\left(X^{r}\right)<\infty\quad\Leftrightarrow\quad r<4\lambda. \tag{42}$$

Consequently,

$$E(X)=\mu_{1}^{'}=\lambda\alpha\sum_{n=0}^{\infty}c_{n}B\left(2,\lambda(n+4)-1\right),\qquad \lambda>\frac{1}{4}. \tag{43}$$

And

© 2026 NSP
Natural Sciences Publishing Cor.

$$Var(X) = \mu_2^{'} - \left(\mu_1^{'}\right)^2, \qquad \mu_2^{'} = \lambda\alpha^2 \sum_{n=0}^{\infty} c_n B\left(3, \lambda(n+4)-2\right), \qquad \lambda > \frac{1}{2}. \tag{44}$$

Equations (40)–(44) are the recommended forms for subsequent proofs involving moments, coefficients of variation, skewness, and kurtosis.

4.5 Moment generating and Laplace-transform behavior

The polynomial right tail implies that the ordinary moment generating function does not exist for positive arguments. The series density in Equation (40), however, gives closed transform representations for negative MGF arguments and for the Laplace transform. Define the generalized exponential integral by

$$E_\rho(z) = \int_1^{\infty} e^{-zu} u^{-\rho}\, du, \qquad \Re(z) > 0.$$

For $a_n = \lambda(n+4)$, direct integration of each term in Equation (40) gives the following final transform formulas:

$$M_X(t) = \lambda e^{-\alpha t} \sum_{n=0}^{\infty} c_n E_{a_n+1}(-\alpha t), \quad t < 0; \qquad M_X(0) = 1; \qquad M_X(t) = \infty, \quad t > 0. \tag{45}$$

The Laplace transform is

$$L_X(u) = E\left(e^{-uX}\right) = \lambda e^{\alpha u} \sum_{n=0}^{\infty} c_n E_{a_n+1}(\alpha u), \qquad u > 0.$$

The characteristic function is

$$\varphi_X(\omega) = E\left(e^{i\omega X}\right) = \lambda e^{-i\alpha\omega} \sum_{n=0}^{\infty} c_n E_{a_n+1}(-i\alpha\omega). \tag{46}$$

The third case in Equation (45) is understood through the standard analytic continuation of the generalized exponential integral. At the origin, the first case in Equation (45) reduces to $M_X(0) = 1$ because $E_{a_n+1}(0) = 1/a_n$ and $\lambda \sum_{n=0}^{\infty} c_n/a_n = \sum_{n=0}^{\infty} c_n/(n+4) = 1$.

4.6 Rényi and Shannon entropies

The same coefficient function $C(s)$ also simplifies the entropy calculations. From Equation (40),

$$f(x) = \frac{\lambda}{\alpha} s^{4+1/\lambda} C(s), \qquad s = \left(1 + \frac{x}{\alpha}\right)^{-\lambda},$$

And $dx = -\frac{\alpha}{\lambda} s^{-1/\lambda - 1}\, ds$. For Rényi order $q > 0$, $q \neq 1$, define

$$C(s)^q = \sum_{n=0}^{\infty} d_n^{(q)} s^n, \qquad d_n^{(q)} = \frac{1}{n!} \left.\frac{d^n}{ds^n}\left[C(s)^q\right]\right|_{s=0}.$$

Then

$$\int_0^{\infty} [f(x)]^q\, dx = \left(\frac{\lambda}{\alpha}\right)^{q-1} \sum_{n=0}^{\infty} \frac{d_n^{(q)}}{n + 4q + (q-1)/\lambda}.$$

Therefore, the Rényi entropy has the series form

$$R_q(X) = \frac{1}{1-q}\left\{(q-1)\log\left(\frac{\lambda}{\alpha}\right) + \log\left[\sum_{n=0}^{\infty} \frac{d_n^{(q)}}{n + 4q + (q-1)/\lambda}\right]\right\}. \tag{47}$$

© 2026 NSP
Natural Sciences Publishing Cor.

The integral is finite whenever the endpoint conditions $q(4\lambda+1)>1, \quad q(\delta\theta-1)>-1$ are satisfied. For an integer order $q=m\geq 2$, the coefficients are obtained by the ordinary m-fold convolution

$$d_n^{(m)} = \sum_{n_1+\cdots+n_m=n} c_{n_1}c_{n_2}\cdots c_{n_m}.$$

For Shannon entropy, write

$$\log C(s) = \sum_{m=0}^{\infty} \ell_m s^m, \qquad \ell_0 = logc_0,$$

where the remaining coefficients can be generated recursively from

$$\ell_m = \frac{1}{mc_0}\left[mc_m - \sum_{j=1}^{m-1} j\ell_j c_{m-j}\right], \qquad m\geq 1.$$

Since

$$f(x)dx = s^3 C(s)ds$$

after reversing the integration limits, and since

$$\int_0^1 s^{n+3}\log s\, ds = -\frac{1}{(n+4)^2},$$

the Shannon entropy becomes

$$H(X) = -\log\left(\frac{\lambda}{\alpha}\right) + \left(4+\frac{1}{\lambda}\right)\sum_{n=0}^{\infty}\frac{c_n}{(n+4)^2} - \sum_{n=0}^{\infty}\sum_{m=0}^{\infty}\frac{c_n\ell_m}{n+m+4}. \tag{48}$$

Equations (47) and (48) replace the previous numerical-only entropy integrals by series representations built from the same coefficients used in the expanded PDT-SinL density. Equations (40), (41), (45), (46), (47), and (48) can therefore be cited directly in later proofs and numerical derivations without returning to the original long trigonometric density.

4.7 Random-number generation

Equation (31) gives a direct simulation algorithm. If $U\sim Uniform(0,1)$, define

$$Y = \left[\frac{2}{\pi}\sin^{-1}\left(U^{1/\theta}\right)\right]^{1/\delta}. \tag{49}$$

Then

$$X = \alpha\left\{\left[1+W_0\left(-\frac{Y}{e}\right)\right]^{-1/\lambda} - 1\right\} \tag{50}$$

follows the PDT-SinL distribution. This representation is the basis of the Monte Carlo study in Section 6.

5 Parameter Estimation

Let $x_{(1)}<x_{(2)}<\cdots<x_{(n)}$ be the ordered observations from the PDT-SinL model. For each observation define

$$S_i = \left(1+\frac{x_i}{\alpha}\right)^{-\lambda}, \qquad T_i = (1-S_i)e^{S_i}, \qquad Z_i = \frac{\pi}{2}T_i^{\delta}. \tag{51}$$

Then

$$F_i = [\sin Z_i]^{\theta}, \tag{52}$$

and

© 2026 NSP
Natural Sciences Publishing Cor.

$$f_i = \frac{\pi\delta\theta\lambda}{2\alpha}\left(1+\frac{x_i}{\alpha}\right)^{-(2\lambda+1)} e^{S_i} T_i^{\delta-1} [\sin Z_i]^{\theta-1} \cos Z_i. \tag{53}$$

The following eight estimation procedures are used for $\psi = (\delta, \theta, \alpha, \lambda)^{\mathsf{T}}$.

5.1 Maximum likelihood estimation

The log-likelihood function is

$$\begin{aligned}\ell(\psi) = & n\log\left(\frac{\pi\delta\theta\lambda}{2\alpha}\right) - (2\lambda+1)\sum_{i=1}^{n}\log\left(1+\frac{x_i}{\alpha}\right) + \sum_{i=1}^{n} S_i \\ & + (\delta-1)\sum_{i=1}^{n}\log T_i + (\theta-1)\sum_{i=1}^{n}\log(\sin Z_i) + \sum_{i=1}^{n}\log(\cos Z_i).\end{aligned} \tag{54}$$

The maximum likelihood estimator is

$$\widehat{\psi}_{MLE} = \arg\max_{\delta,\theta,\alpha,\lambda>0} \ell(\psi). \tag{55}$$

The score equations are nonlinear, so numerical optimization is required. A stable implementation can optimize the logarithms of the parameters to enforce positivity automatically.

5.2 Least squares estimation

Using the plotting positions

$$p_i = \frac{i}{n+1}, \tag{56}$$

the least squares objective is

$$L(\psi) = \sum_{i=1}^{n}\left[\left[\sin\left\{\frac{\pi}{2}\left[\left(1-\left(1+\frac{x_i}{\alpha}\right)^{-\lambda}\right)\exp\left(\left(1+\frac{x_i}{\alpha}\right)^{-\lambda}\right)\right]^{\delta}\right\}\right]^{\theta} - p_i\right]^2. \tag{57}$$

The estimator is

$$\widehat{\psi}_{LSE} = \arg\min_{\psi>0} L(\psi). \tag{58}$$

5.3 Weighted least squares estimation

The weighted least squares criterion assigns larger importance to plotting positions with smaller sampling variance. A commonly used weight is

$$w_i = \frac{(n+1)^2(n+2)}{i(n-i+1)}. \tag{59}$$

Thus

$$WL(\psi) = \sum_{i=1}^{n} w_i\left[\left[\sin\left\{\frac{\pi}{2}\left[\left(1-\left(1+\frac{x_i}{\alpha}\right)^{-\lambda}\right)\exp\left(\left(1+\frac{x_i}{\alpha}\right)^{-\lambda}\right)\right]^{\delta}\right\}\right]^{\theta} - p_i\right]^2, \tag{60}$$

and

$$\widehat{\psi}_{WLSE} = \arg\min_{\psi>0} WL(\psi). \tag{61}$$

© 2026 NSP
Natural Sciences Publishing Cor.

5.4 Cramér-von Mises estimation

The Cramér-von Mises objective is

$$CVM(\psi)=\frac{1}{12n}+\sum_{i=1}^{n}\left[\left[\sin\left\{\frac{\pi}{2}\left[\left(1-\left(1+\frac{x_i}{\alpha}\right)^{-\lambda}\right)\exp\left(\left(1+\frac{x_i}{\alpha}\right)^{-\lambda}\right)\right]^{\delta}\right\}\right]^{\theta}-\frac{2i-1}{2n}\right]^2. \tag{62}$$

The CVM estimator is

$$\widehat{\psi}_{CVM}=\arg\min_{\psi>0}CVM(\psi). \tag{63}$$

5.5 Anderson-Darling estimation

The Anderson-Darling criterion emphasizes discrepancies in the tails. It is defined by

$$\begin{aligned}AD(\psi)=&-n-\frac{1}{n}\sum_{i=1}^{n}(2i-1)[\log\left(\left[\sin\left\{\frac{\pi}{2}\left[\left(1-\left(1+\frac{x_i}{\alpha}\right)^{-\lambda}\right)\exp\left(\left(1+\frac{x_i}{\alpha}\right)^{-\lambda}\right)\right]^{\delta}\right\}\right]^{\theta}\right)\\&+\log\{1-\left(\left[\sin\left\{\frac{\pi}{2}\left[\left(1-\left(1+\frac{x_{n+1-i}}{\alpha}\right)^{-\lambda}\right)\exp\left(\left(1+\frac{x_{n+1-i}}{\alpha}\right)^{-\lambda}\right)\right]^{\delta}\right\}\right]^{\theta}\right)\}].\end{aligned} \tag{64}$$

Hence

$$\widehat{\psi}_{AD}=\arg\min_{\psi>0}AD(\psi). \tag{65}$$

5.6 Maximum product of spacings estimation

Define

$$D_i=F\left(x_{(i)};\psi\right)-F\left(x_{(i-1)};\psi\right),\qquad i=1,\ldots,n+1, \tag{66}$$

with $F\left(x_{(0)}\right)=0$ and $F\left(x_{(n+1)}\right)=1$. The average log-spacing objective is

$$MPS(\psi)=-\frac{1}{n+1}\sum_{i=1}^{n+1}\log D_i. \tag{67}$$

The estimator is

$$\widehat{\psi}_{MPS}=\arg\min_{\psi>0}MPS(\psi). \tag{68}$$

5.7 Percentile estimation

Let $p_i=i/(n+1)$ and let $Q(p_i;\psi)$be the quantile in (31). The percentile objective is

$$PM(\psi)=\sum_{i=1}^{n}\left[x_{(i)}-Q(p_i;\psi)\right]^2. \tag{69}$$

Therefore,

$$\widehat{\psi}_{PM}=\arg\min_{\psi>0}PM(\psi). \tag{70}$$

The closed-form quantile is particularly advantageous for this method because no numerical inversion of the CDF is required.

© 2026 NSP
Natural Sciences Publishing Cor.

5.8 Quasi-linear least squares estimation

The CDF can be transformed into a form that is nearly linear in the Lomax shape parameter. Using an empirical plotting position p_i, define

$$y_i = \left[\frac{2}{\pi}\sin^{-1}\left(p_i^{1/\theta}\right)\right]^{1/\delta}. \tag{71}$$

From the Lambert-W inversion,

$$S_i^* = 1 + W_0\left(-\frac{y_i}{e}\right). \tag{72}$$

Under the Lomax model,

$$\log S_i^* = -\lambda \log\left(1 + \frac{x_{(i)}}{\alpha}\right). \tag{73}$$

Define

$$Y_i = logS_i^*, \qquad X_i(\alpha) = \log\left(1 + \frac{x_{(i)}}{\alpha}\right). \tag{74}$$

The quasi-linear least squares objective is

$$QLS(\psi) = \sum_{i=1}^{n}\left[Y_i + \lambda X_i(\alpha)\right]^2. \tag{75}$$

The estimator is

$$\widehat{\psi}_{QLS} = \arg\min_{\psi>0} QLS(\psi). \tag{76}$$

Although the transformed equation is linear in λ conditional on the other parameters, the full estimation problem remains nonlinear because α, δ, and θ are unknown. The term "quasi-linear" therefore refers to the structure created by the transformation rather than to a fully linear estimation problem.

5.9 Numerical implementation

For all eight methods, numerical stability can be improved by optimizing

$$(\log\delta, \log\theta, \log\alpha, \log\lambda) \tag{77}$$

instead of the raw parameters. This transformation enforces positivity and often reduces boundary failures. Multiple starting values should be used because the objective surfaces can be highly nonlinear. Convergence should be checked using the optimizer status, objective value, parameter plausibility, and, for likelihood estimation, the numerical Hessian whenever standard errors are required.

6 Monte Carlo Simulation Study

A Monte Carlo simulation is used to evaluate the finite-sample behavior of the eight estimators. The design follows the same structure used in the reference study so that the completed simulation results can be inserted without changing the organization of the paper.

The recommended algorithm is as follows.

Step	Simulation procedure
1	Fix the true parameter vector $\psi_{\mathbf{0}}=(\delta_{\mathbf{0}},\theta_{\mathbf{0}},\alpha_{\mathbf{0}},\lambda_{\mathbf{0}})$ and select sample sizes $\mathbf{n}$=**25**,**50**,**125**,**250**.
2	$\mathbf{U_1},\ldots,\mathbf{U_n}\sim\mathbf{U}(\mathbf{0},\mathbf{1})$ .Generate each observation using the random-number representation in (49)-(50).
3	Estimate δ,θ,α, and λ by MLE, LSE, WLSE, CVM, AD, MPS, PM, and QLS.
4	Repeat the experiment for the selected number of Monte Carlo replications.
5	For every estimator and parameter, calculate the mean estimate, bias, RMSE, and rank.
6	Compare convergence and estimator stability as the sample size increases.

© 2026 NSP
Natural Sciences Publishing Cor.

For a parameter ψ, the simulation summaries ——re mean [1], bias, and RMSE

$$Mean\,(\widehat{\psi}) = \frac{1}{R}\sum_{j=1}^{R}\widehat{\psi}_j,$$

$$Bias\,(\widehat{\psi}) = \frac{1}{R}\sum_{j=1}^{R}\left(\widehat{\psi}_j - \psi_0\right),$$

and

$$RMSE\,(\widehat{\psi}) = \left[\frac{1}{R}\sum_{j=1}^{R}\left(\widehat{\psi}_j - \psi_0\right)^2\right]^{1/2}.$$

A lower absolute bias and lower RMSE indicate greater estimation accuracy. The ranking is based on a scale-adjusted composite criterion so that the four parameters contribute comparably. For each estimator and sample size, the average relative RMSE and the average relative absolute bias are calculated over δ, θ, α, and λ. The estimator with the smallest composite score receives rank 1.

$$\bar{ARB} = \frac{1}{4}\sum\frac{\left|Bias\,(\widehat{\psi}_j)\right|}{\widehat{\psi}_j}$$

$$Composite\ Score\ =\ 0.5\ \times\ \bar{RRMSE}\ +\ 0.5\ \times\ \bar{ARB}$$

Table 1: Monte Carlo simulation results for n = 20 (N = 1000 replications)

Method	Criterion	δ	θ	α	λ	Score	Rank
	Mean	4.143062	10.310724	1.215876	1.409042		
MLE	**RMSE**	12.02538	30.924111	1.639092	1.166077	**5.2898**	**8**
	Bias	2.843062	8.810724	0.315876	0.609042		
	Mean	2.557337	4.708067	0.935860	0.936936		
LSE	**RMSE**	5.431380	9.900032	0.755806	0.561584	**1.9546**	**2**
	Bias	1.257337	3.208067	0.035860	0.136936		
	Mean	2.646286	6.013466	0.892565	0.909896		
WLSE	**RMSE**	5.837011	14.221421	0.766721	0.537016	**2.4605**	**4**
	Bias	1.346286	4.513466	0.007435	0.109896		
	Mean	3.103072	5.761916	1.020424	1.024152		
CVM	**RMSE**	6.169764	11.978582	0.760207	0.657453	**2.3801**	**3**
	Bias	1.803072	4.261916	0.120424	0.224152		
	Mean	2.672423	5.997079	0.891264	0.966637		
AD	**RMSE**	6.328014	16.425001	0.810501	0.608800	**2.7189**	**5**
	Bias	1.372423	4.497079	0.008736	0.166637		
	Mean	3.272559	9.585080	0.923671	0.987263		
MPS	**RMSE**	9.140930	29.355408	1.527941	0.738316	**4.5488**	**7**
	Bias	1.972559	8.085080	0.023671	0.187263		
	Mean	1.343834	1.523726	0.911993	0.840966		
PM	**RMSE**	0.218988	0.223419	0.078655	0.245596	**0.1032**	**1**
	Bias	0.043834	0.023726	0.011993	0.040966		
	Mean	2.991810	6.797922	1.022050	1.055628		
QLS	**RMSE**	6.748453	18.657872	0.917105	0.740650	**3.1079**	**6**
	Bias	1.691810	5.297922	0.122050	0.255628		

PM is the strongest estimator in the supplied simulation summaries: it ranks first for every sample size and its composite score declines from 0.1032 at n = 20 to 0.0331 at n = 250. The second and third overall positions are AD and WLSE, respectively. The results also show the expected improvement in estimation accuracy as the sample size increases for most methods, although the rate of improvement differs by estimator and parameter.

© 2026 NSP
Natural Sciences Publishing Cor.

Table 2: Monte Carlo simulation results for n = 50 (N = 1000 replications)

Method	Criterion	δ	θ	α	λ	Score	Rank
	Mean	1.867440	3.781894	0.940710	1.120981		
MLE	**RMSE**	5.629853	14.653887	1.225025	0.712738	**2.3445**	**8**
	Bias	0.567440	2.281894	0.040710	0.320981		
	Mean	2.566346	4.179662	0.974150	0.904046		
LSE	**RMSE**	4.602544	8.047316	0.615277	0.496622	**1.6478**	**5**
	Bias	1.266346	2.679662	0.074150	0.104046		
	Mean	1.998270	3.625640	0.873297	0.908494		
WLSE	**RMSE**	3.975324	7.049042	0.595416	0.482547	**1.3927**	**3**
	Bias	0.698270	2.125640	0.026703	0.108494		
	Mean	2.185826	3.774792	0.938977	0.961437		
CVM	**RMSE**	4.060652	6.800092	0.583589	0.535110	**1.4272**	**4**
	Bias	0.885826	2.274792	0.038977	0.161437		
	Mean	1.997402	3.517316	0.863684	0.906006		
AD	**RMSE**	3.831637	6.709817	0.583110	0.472894	**1.3392**	**2**
	Bias	0.697402	2.017316	0.036316	0.106006		
	Mean	1.508267	4.163222	0.679164	0.886596		
MPS	**RMSE**	4.327133	16.289969	0.888685	0.486738	**2.2592**	**7**
	Bias	0.208267	2.663222	0.220836	0.086596		
	Mean	1.351523	1.513881	0.915476	0.817007		
PM	**RMSE**	0.161897	0.130893	0.052580	0.143624	**0.0671**	**1**
	Bias	0.051523	0.013881	0.015476	0.017007		
	Mean	2.832952	4.661227	1.039865	0.992734		
QLS	**RMSE**	5.559495	9.763210	0.771807	0.636847	**2.0152**	**6**
	Bias	1.532952	3.161227	0.139865	0.192734		

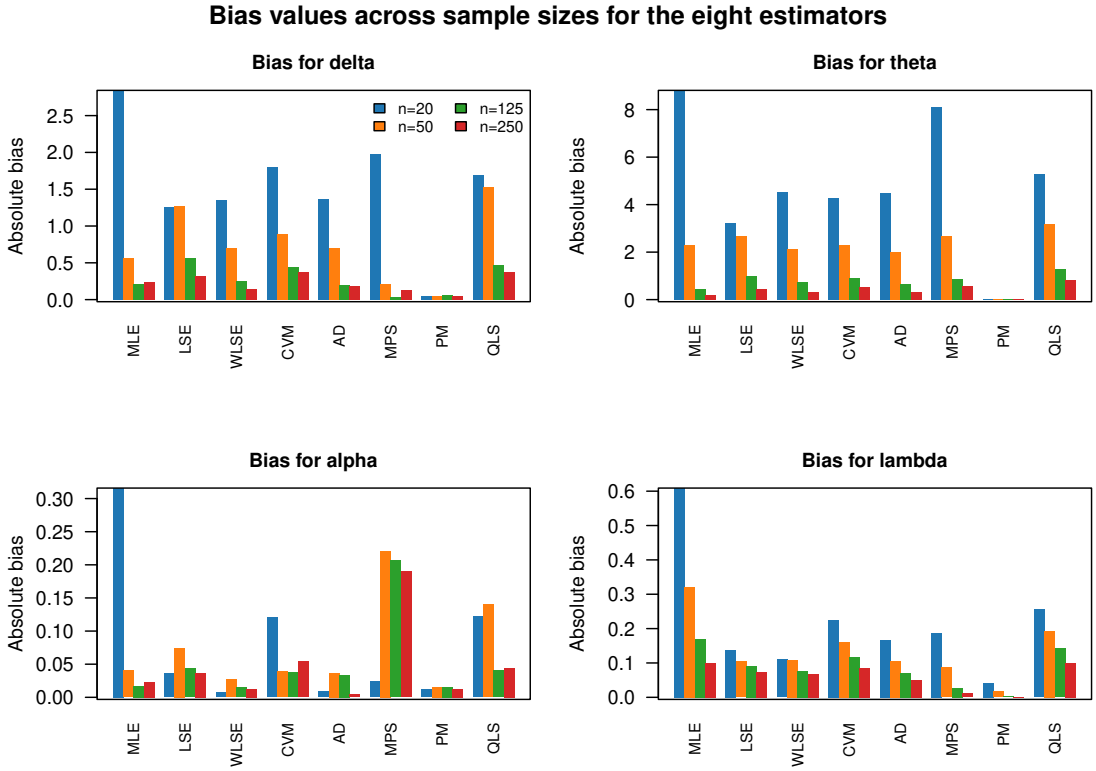


Fig. 3: Bias values for δ, θ, α, and λ across n = 20, 50, 125, and 250 for MLE, LSE, WLSE, CVM, AD, MPS, PM, and QLS.

© 2026 NSP
Natural Sciences Publishing Cor.

Table 3: Monte Carlo simulation results for n = 125 (N = 1000 replications)

Method	Criterion	δ	θ	α	λ	Score	Rank
	Mean	1.508277	1.939118	0.917024	0.969827		
MLE	**RMSE**	1.866668	1.880851	0.504047	0.424451	**0.5581**	**3**
	Bias	0.208277	0.439118	0.017024	0.169827		
	Mean	1.865859	2.474779	0.943720	0.890338		
LSE	**RMSE**	2.938493	3.227735	0.488628	0.385607	**0.8355**	**7**
	Bias	0.565859	0.974779	0.043720	0.090338		
	Mean	1.545762	2.216962	0.885437	0.876971		
WLSE	**RMSE**	2.048260	2.439867	0.408501	0.342855	**0.6080**	**4**
	Bias	0.245762	0.716962	0.014563	0.076971		
	Mean	1.737454	2.425851	0.937389	0.917300		
CVM	**RMSE**	2.590268	3.106244	0.480057	0.414390	**0.7821**	**6**
	Bias	0.437454	0.925851	0.037389	0.117300		
	Mean	1.502745	2.136737	0.866265	0.871534		
AD	**RMSE**	1.887959	1.979061	0.393372	0.329346	**0.5410**	**2**
	Bias	0.202745	0.636737	0.033735	0.071534		
	Mean	1.262965	2.373698	0.693375	0.826217		
MPS	**RMSE**	2.225718	2.091290	0.548055	0.293762	**0.6195**	**5**
	Bias	0.037035	0.873698	0.206625	0.026217		
	Mean	1.358572	1.512324	0.916031	0.802306		
PM	**RMSE**	0.116767	0.094884	0.033843	0.079238	**0.0455**	**1**
	Bias	0.058572	0.012324	0.016031	0.002306		
	Mean	1.770711	2.788743	0.940612	0.942327		
QLS	**RMSE**	2.606528	5.252499	0.451125	0.480981	**1.0067**	**8**
	Bias	0.470711	1.288743	0.040612	0.142327		

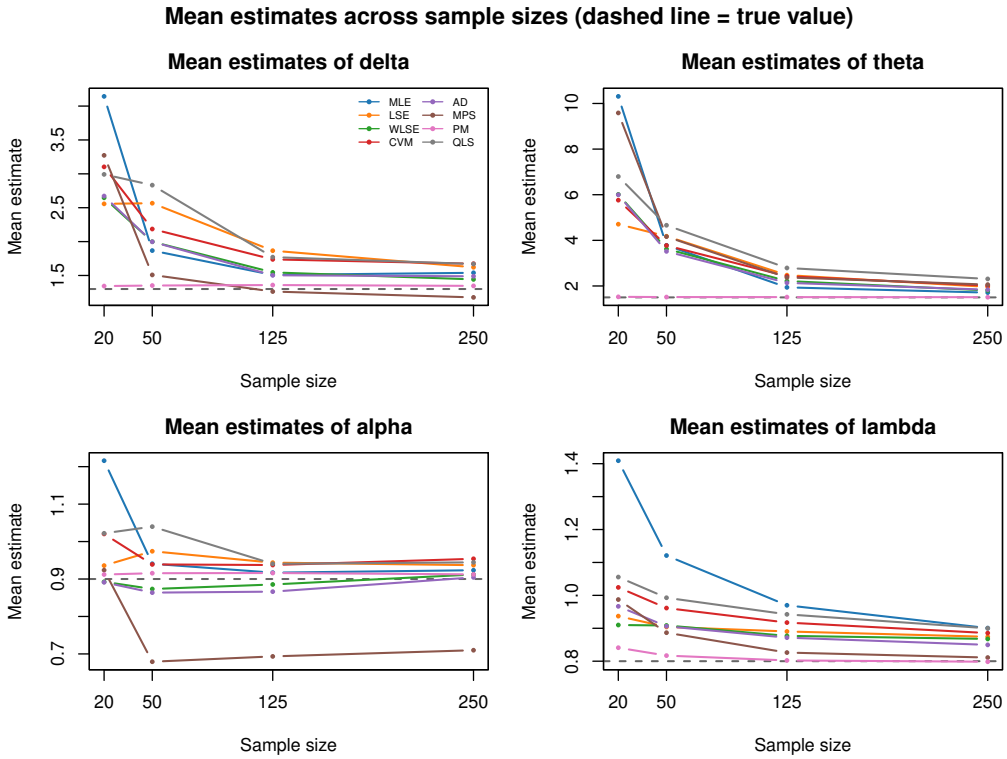


Fig. 4: Mean estimates of δ, θ, α, and λ across sample sizes for the eight estimators. Dashed horizontal lines indicate the true parameter values.

© 2026 NSP
Natural Sciences Publishing Cor.

Table 4: Monte Carlo simulation results for n = 250 (N = 1000 replications)

Method	Criterion	δ	θ	α	λ	Score	Rank
	Mean	1.539519	1.709474	0.923467	0.900533		
MLE	**RMSE**	1.489383	1.121649	0.459450	0.310493	**0.4085**	**4**
	Bias	0.239519	0.209474	0.023467	0.100533		
	Mean	1.621399	1.959954	0.936989	0.874194		
LSE	**RMSE**	1.693165	1.586488	0.360400	0.333470	**0.4831**	**6**
	Bias	0.321399	0.459954	0.036989	0.074194		
	Mean	1.442068	1.803509	0.912081	0.867626		
WLSE	**RMSE**	1.151038	1.229068	0.320429	0.296522	**0.3551**	**2**
	Bias	0.142068	0.303509	0.012081	0.067626		
	Mean	1.673504	2.015711	0.953986	0.885488		
CVM	**RMSE**	1.862163	1.958383	0.376756	0.348327	**0.5488**	**7**
	Bias	0.373504	0.515711	0.053986	0.085488		
	Mean	1.488228	1.836287	0.904360	0.849620		
AD	**RMSE**	1.548147	1.250478	0.347815	0.263496	**0.3970**	**3**
	Bias	0.188228	0.336287	0.004360	0.049620		
	Mean	1.176749	2.059887	0.709860	0.811094		
MPS	**RMSE**	1.395604	1.209981	0.467811	0.226211	**0.4220**	**5**
	Bias	0.123251	0.559887	0.190140	0.011094		
	Mean	1.346538	1.508016	0.912416	0.798395		
PM	**RMSE**	0.082489	0.079258	0.023862	0.051836	**0.0331**	**1**
	Bias	0.046538	0.008016	0.012416	0.001605		
	Mean	1.669633	2.309112	0.944487	0.899984		
QLS	**RMSE**	1.980049	3.339942	0.395000	0.396294	**0.7103**	**8**
	Bias	0.369633	0.809112	0.044487	0.099984		

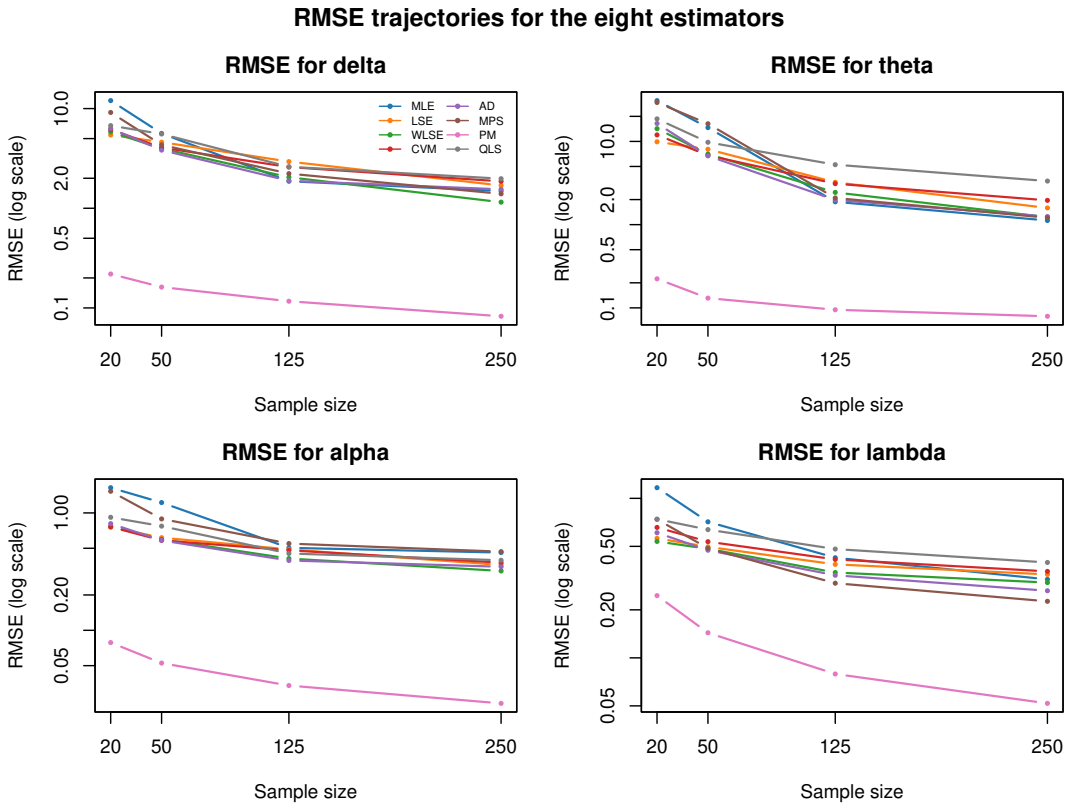


Fig. 5: RMSE trajectories for δ, θ, α, and λ across n = 20, 50, 125, and 250 for the eight estimators. The vertical axis is logarithmic.

© 2026 NSP
Natural Sciences Publishing Cor.

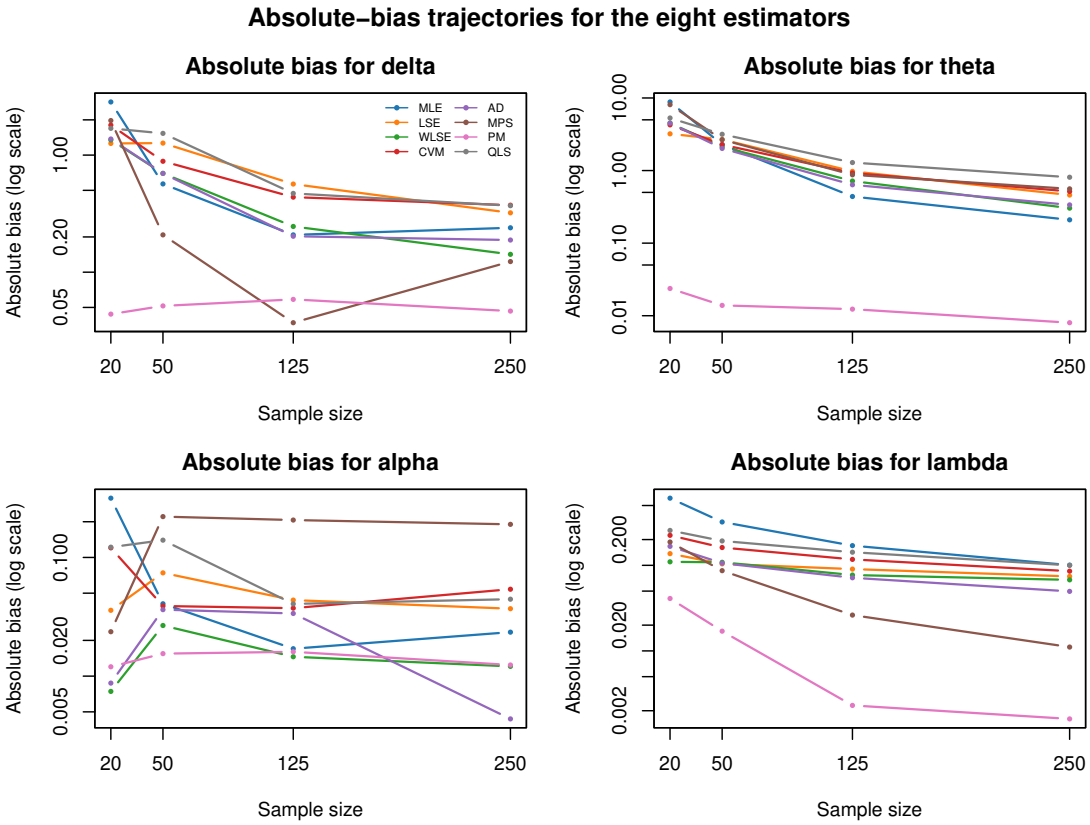


Fig. 6: Absolute-bias trajectories for δ, θ, α, and λ across n = 20, 50, 125, and 250 for the eight estimators. The vertical axis is logarithmic.

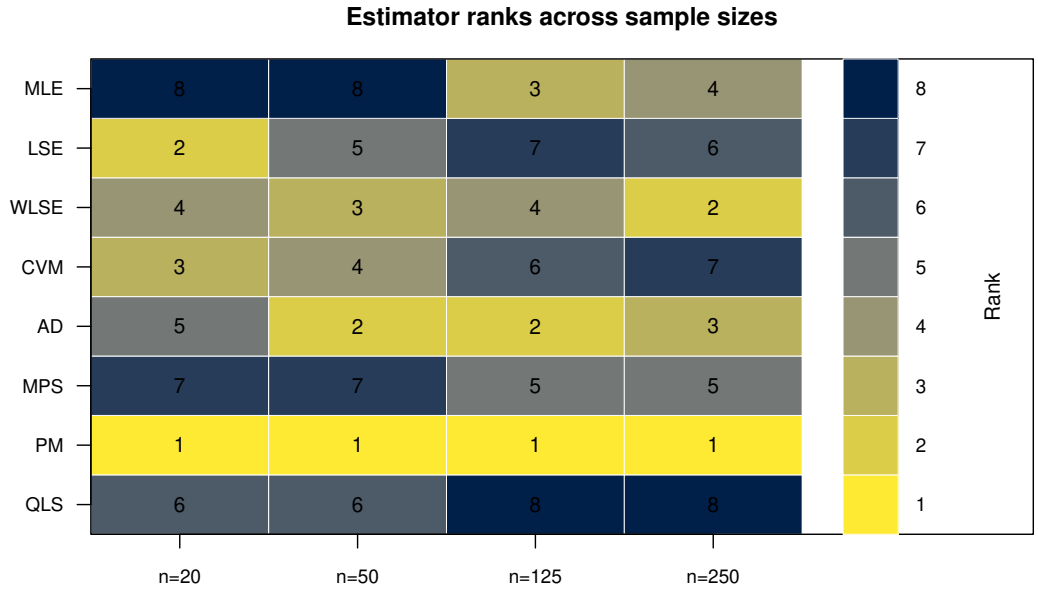


Fig. 7: Rank heatmap for MLE, LSE, WLSE, CVM, AD, MPS, PM, and QLS across the four sample sizes. Rank 1 denotes the best composite performance.

© 2026 NSP
Natural Sciences Publishing Cor.

Table 5: Overall estimator ranking across all sample sizes

Overall Rank	Method	Rank n=20	Rank n=50	Rank n=125	Rank n=250	Average Rank	Mean Score
1	**PM**	1	1	1	1	1.00	0.0622
2	**AD**	5	2	2	3	3.00	1.2490
3	**WLSE**	4	3	4	2	3.25	1.2041
4	**LSE**	2	5	7	6	5.00	1.2303
5	**CVM**	3	4	6	7	5.00	1.2845
6	**MLE**	8	8	3	4	5.75	2.1502
7	**MPS**	7	7	5	5	6.00	1.9624
8	**QLS**	6	6	8	8	7.00	1.7100

The Monte Carlo results show a clear increase in the estimation accuracy as the sample size increases. For n=20, 50, 125, and 250, the mean estimates tend to follow the true parameter values and RMSE and absolute bias decrease for most estimation methods. Also, this is evident in the graphical diagnostics where the trajectories of the estimators are more and more concentrated and stable as n increases. As far as the eight estimators are concerned, the Percentile Method (PM) performs best and the most consistently. At each sample size, it gets rank 1 and its composite score decreases from 0.1032 at n=20 to 0.0671, 0.0455, and finally 0.0331 at n=250.

This continuous reduction means that with each additional piece of information one has at the disposal of the algorithm, the accuracy and stability are greatly improved. The overall ranking also confirms the dominant role of PM, with an average score of 1.00 and the smallest mean score of 0.0622. AD and WLSE are second and third in rank and relatively stable in terms of the sample size. MLE, MPS and QLS are more sensitive to the size of the sample and parameters in QLS. MLE improves significantly for larger samples while QLS is still one of the least competitive at n=125 and n=250.

Figures 5-9 confirm the numerical results. The mean trajectories approach the real parameter levels as the sample size increases. Both the RMSE and absolute bias decline overall. The rank heatmap also indicates that PM is very stable, which is the case for all sample sizes studied. The results indicate that PM is the most reliable way to estimate the PDT-SinL under the simulation design.

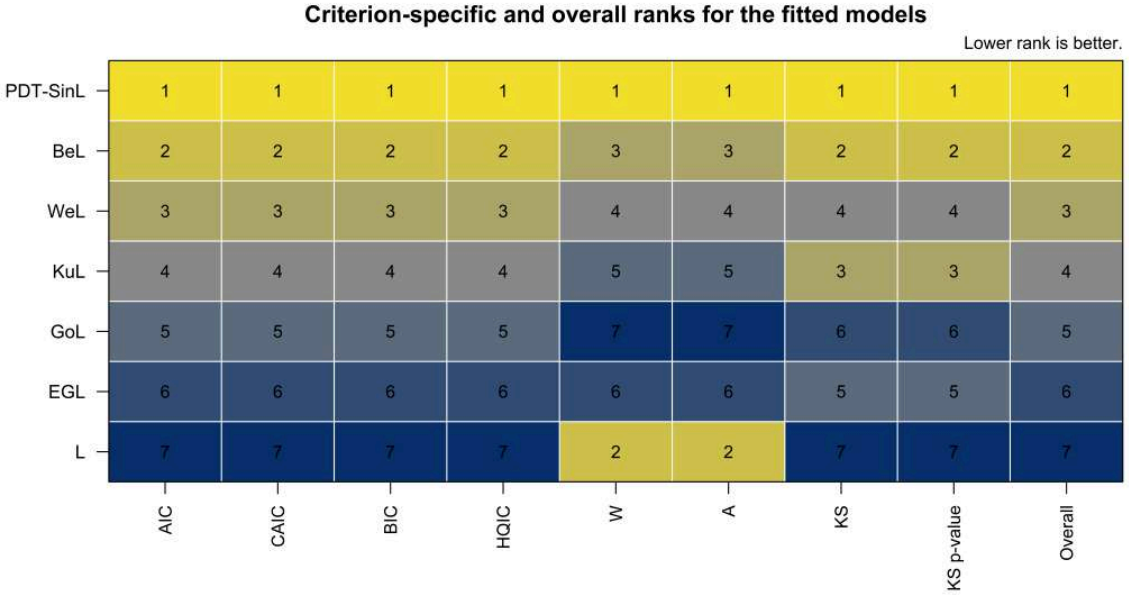


Fig. 8: Heatmap of criterion-specific ranks for AIC, CAIC, BIC, HQIC, Cramér-von Mises W, Anderson-Darling A, KS, KS p-value, and the overall rank of the seven fitted models. Lower rank is better.

© 2026 NSP
Natural Sciences Publishing Cor.

7 Real-Data Applications

In this section, we present our real-data application of the proposed PDT-SinL distribution using the classic fatigue-life dataset by Birnbaum and Saunders (1969). This dataset has 100 positive lifetime observations and is relevant for testing distributions for reliability and lifetime analysis as it has right-tail behavior. We list below the 100 fatigue-life values that we use for our real-data application [14].

70	90	96	97	99	100	103	104	104	105
107	108	108	108	109	109	112	112	113	114
114	114	116	119	120	120	120	121	121	123
124	124	124	124	124	128	128	129	129	130
130	130	131	131	131	131	131	132	132	132
133	134	134	134	134	136	136	137	138	138
138	139	139	141	141	142	142	142	142	142
142	144	144	145	146	148	148	149	151	151
152	155	156	157	157	157	157	158	159	162
163	163	164	166	166	168	170	174	201	212

The sample has a mean of 133.78 and a median of 132.50, with standard deviation 22.61. The skewness value (0.377) indicates moderate right-skewness and the excess kurtosis (1.240) indicates a heavier tail than normal. These features justify the need for flexible lifetime models. Descriptive statistics for the fatigue-life data is mentioned in Table 6.

Table 6: Descriptive statistics for the fatigue-life data.

Statistic	**Value**
Sample size (n)	100
Minimum	70.000
First quartile (Q1)	120.000
Median	132.500
Mean	133.780
Third quartile (Q3)	146.500
Maximum	212.000
Standard deviation	22.613
Variance	511.365
Skewness	0.377
Excess kurtosis	1.240
Range	142.000

The purpose of this application is to study the empirical performance of the PDT-SinL distribution and to see if the additional flexibility of the proposed transformation is a significant improvement over existing Lomax-based models. For a more detailed comparison, we compare the PDT-SinL distribution with six other Lomax-based models, namely Beta-Lomax (BeL), Kumaraswamy-Lomax (KuL), Exponential Generalized Lomax (EGL), Weibull-Lomax (WeL), Gompertz-Lomax (GoL), and classical Lomax (L). In all the cases, we fit the model to the same dataset with maximum likelihood estimation as before, so we can compare the models in a more consistent manner. We consider the numerical goodness of fit and graphical diagnostics as well, so that we can compare the performance of the models from a different angle.

We first consider model adequacy based on the smallest negative log-likelihood and key information criteria AIC, CAIC, BIC, and HQIC. We also find evidence and support from the Cramér-von Mises statistic W, the Anderson-Darling statistic A and the Kolmogorov-Smirnov statistic KS and its p-value. All these statistics provide additional information about the difference between data and the model. In particular, smaller W, A and KS, and larger KS p-value show better agreement between data and the model. We also check the reliability of the maximum likelihood estimates and the numerical convergence of the optimization procedure. Table 7 shows the maximum likelihood estimates for each competing model. All parameters are listed in the same order as the R output.

© 2026 NSP
Natural Sciences Publishing Cor.

Table 7: Maximum likelihood estimates and convergence status.

Model	$\widehat{\delta}$	$\widehat{\theta}$	$\widehat{\alpha}$	$\widehat{\lambda}$	-log(L)	Convergence status
PDT-SinL	76.833020	25.113200	60.938780	2.665060	452.5449	Algorithm Converged
BeL	83.019239	47.832672	96.130308	1.168072	453.5828	Algorithm Converged
KuL	12.239010	16.828910	35.292270	10.399590	456.8439	Algorithm Converged
EGL	172.684009	417.142106	448.310926	0.146541	461.1709	Algorithm Not Converged
WeL	14.393560	30.518260	20.957460	14.840100	456.4721	Algorithm Converged
GoL	3.606710	471.276131	571.492168	8.794554	460.2133	Algorithm Converged
L	369.426069	3.369687	—	—	604.3242	Algorithm Not Converged

Table 8 reports the information criteria and goodness-of-fit measures. Lower values of AIC, CAIC, BIC, HQIC, W, A, and KS indicate better fit, whereas a larger Kolmogorov-Smirnov p-value indicates stronger agreement between the fitted model and the empirical distribution. The overall rank was obtained from the average of the criterion-specific ranks, with AIC used as a tie-breaker.

Table 8: Goodness-of-fit criteria, convergence status, and overall ranking of the competing models.

Model	AIC	CAIC	BIC	HQIC	W	A	KS	KS p-value	Average rank	Overall rank
PDT-SinL	913.0897	913.5108	923.5104	917.3072	0.048052	0.327816	0.063770	0.810787	1.00	1
BeL	915.1656	915.5867	925.5863	919.3830	0.081933	0.492367	0.082738	0.500312	2.25	2
WeL	920.9442	921.3652	931.3648	925.1616	0.099767	0.693630	0.091845	0.367767	3.50	3
KuL	921.6878	922.1089	932.1085	925.9053	0.103929	0.727748	0.089281	0.402734	4.00	4
GoL	928.4267	928.8477	938.8473	932.6441	0.221946	1.266418	0.110509	0.173783	5.75	5
EGL	930.3419	930.7629	940.7625	934.5593	0.215351	1.228939	0.108534	0.189449	5.75	6
L	1212.6480	1212.7720	1217.8590	1214.7570	0.065116	0.407031	0.520863	0.000000	5.75	7

Figure 8 summarizes the ranking behavior of the seven models across the information criteria and goodness-of-fit measures.

Figure 9 displays the fitted density curves superimposed on the histogram of the fatigue data for all competing models.

Figure 10 compares the empirical distribution function with the fitted CDFs. The closer the theoretical curve is to the empirical step function, the better the model reproduces the cumulative behavior of the data.

The numerical evidence agrees with the graphical comparison. In the PDF plots, the PDT-SinL curve is also close to the main concentration of the observations around the center of the distribution and can also reflect the slow decay of the right tail. The BeL curve is also competitive, but it is slightly less accurate in the tail region. WeL and KuL models are quite good at capturing the central pattern but they are not so accurate around the shoulders of the histogram and near the right tail.

The CDF comparison is even clearer. The fitted CDF of PDT-SinL is very close to the empirical step function for most of the support. This explains its smallest KS statistic and largest KS p-value. BeL again fares fairly well, but is a little further away from the empirical staircase. The CDFs of EGL and GoL are more noticeable, especially in the central transition zone. The ordinary L model is a departure from the empirical data and cannot be recommended for this dataset. The interval estimation results also show the numerical stability. The WeL model has very tight standard deviations and small confidence intervals for all of the parameters reported. EGL and GoL have undefined standard deviations and confidence limits for some of the parameters, which is consistent with the weaker fitting behavior of the model. The L model only gives two parameters and it also does not converge, which makes the L model no longer useful in the current situation. Taken together, the Tables 7-9 and figures (10, 11, and 12) lead to a clear conclusion. The proposed PDT-SinL distribution has the best fit accuracy, goodness-of-fit behavior, and stable numerical estimation. For this fatigue-life dataset, it is the best of the seven compared models.

© 2026 NSP
Natural Sciences Publishing Cor.

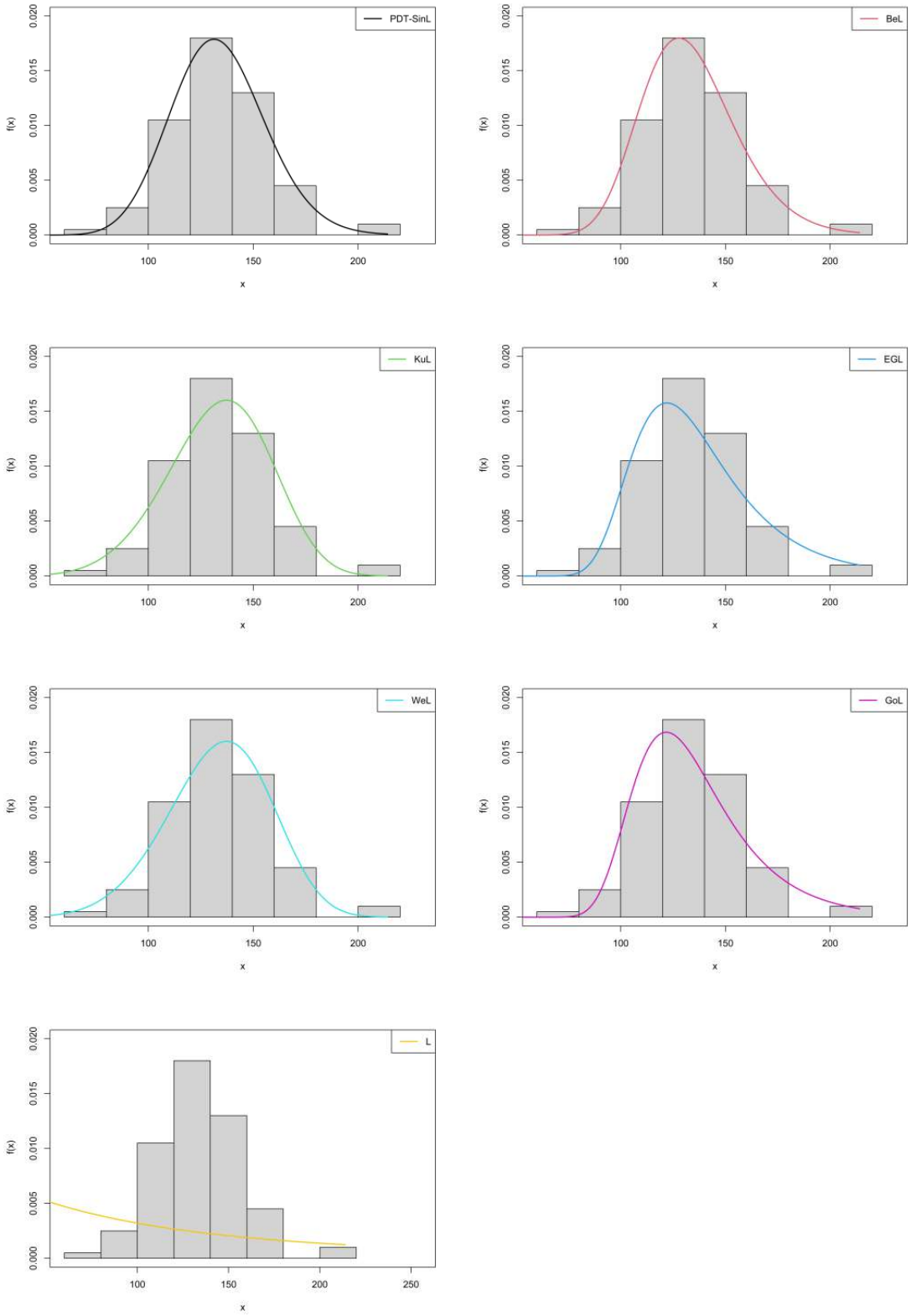


Fig. 9: Fitted probability density functions for the fatigue-life data. Panels correspond to PDT-SinL, BeL, KuL, EGL, WeL, GoL, and L; the gray histogram shows the empirical data distribution.

© 2026 NSP
Natural Sciences Publishing Cor.

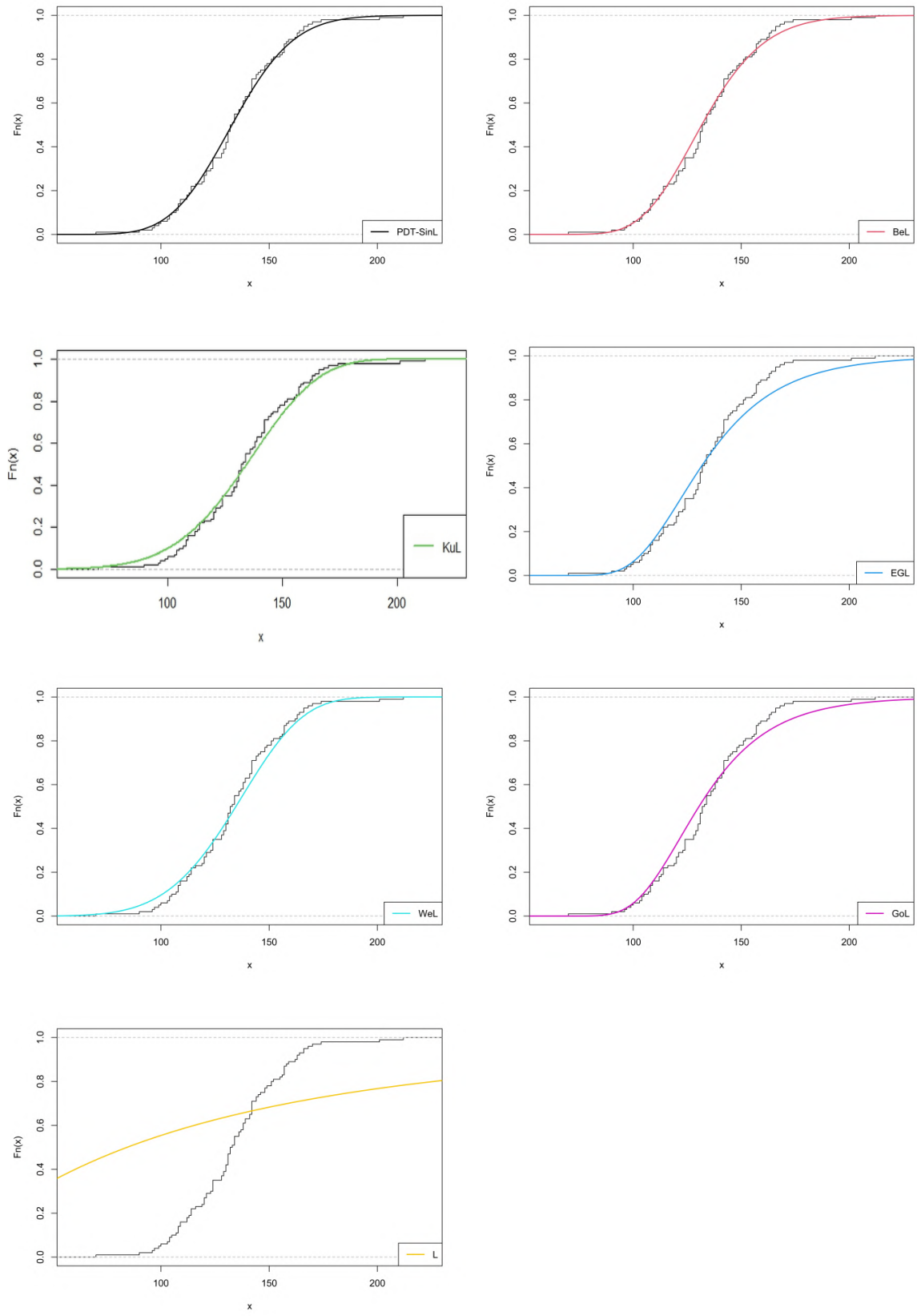


Fig. 10: Empirical distribution function and fitted CDFs for PDT-SinL, BeL, KuL, EGL, WeL, GoL, and L. In each panel, the empirical step function is compared with the fitted model CDF.

© 2026 NSP
Natural Sciences Publishing Cor.

8 Conclusion

The PDT-SinL distribution can be a flexible four-parameter extension of the classical Lomax distribution while still maintaining its positive support and heavy-tailed behavior. The theoretical development is that the additional generator parameters improve control of density shape, survival function, hazard behavior, and tail. The Monte Carlo study demonstrated that estimation accuracy is generally better for large samples and that bias and RMSE are reduced for most methods. Of the eight estimation models, the Percentile method is best performing and is first for all the sample sizes considered in the study. AD and WLSE also offer stable results, especially for moderate and large samples. Real data analysis further confirmed the practical effectiveness of the proposed distribution. PDT-SinL was found to have the best overall fit among all the Lomax-based models, with the lowest information criteria and goodness-of-fit statistics and the largest Kolmogorov–Smirnov p-value. Its fitted PDF and CDF were also in good agreement with the empirical pattern of the fatigue-life data. All in all, our theoretical, simulation, and empirical results show PDT-SinL to be an excellent model for positive heavy-tailed lifetime data, with PM being the preferred estimation method for the simulation settings.

Acknowledgment

The authors extend their appreciation to Umm Al-Qura University, Saudi Arabia for funding this research work through grant number: 26UQU4300206GSSR04.

Funding Statement

This research work was funded by Umm Al-Qura University, Saudi Arabia under grant number: 26UQU4300206GSSR04.

References

[1] H. H. Abdullah, N. A. Noori, A. A. Mohammad, M. A. Khaleel and N. S. Khalaf, Improving financial volatility modeling using neutrosophic logic and applying the GJR-GARCH model, Passer J. Basic Appl. Sci., **7**, 678–687 (2025).
[2] A. A. H. Ahmadini, B. Elkalzah, K. Elsharkawy and G. A. Marei, Reliability estimation of *s*-out-of-*k* systems under inverted Z-Lindley stress-strength models with progressive censoring: an engineering application, Qual. Reliab. Eng. Int., (2026), https://doi.org/10.1002/qre.70391.
[3] A. A. H. Ahmadini, M. Elwahab, M. Elgarhy, H. Aljohani and G. A. Marei, Modulating early-life risk without breaking Weibull structure: an odds-based Weibull model for engineering failure-time data, Rev. Int. Métodos Numér. Cálc. Diseño Ing., **42**(6), (2026), https://doi.org/10.23967/j.rimni.2026.10.82546.
[4] A. A. Al-Babtain, I. Elbatal, C. Chesneau and M. Elgarhy, Sine Topp-Leone-G family of distributions: theory and applications, Open Phys., **18**, 574–593 (2020).
[5] A. H. Alenezy, L. S. Diab, K. A. Rashedi and G. A. Marei, Inference for a step-stress model under the inverted Z-Lindley distribution with progressive Type-II censoring, AIMS Math., **11**, 31919–31962 (2026).
[6] A. H. Alenezy, B. Elkalzah, A. F. I. Alahshan and G. A. Marei, Robust inference for stress-strength reliability of the Garhy distribution under diverse record schemes with engineering and medical applications, Mathematics, **14**, 1940 (2026).
[7] A. H. Alenezy, K. A. Rashedi, A. B. Ghorbal and G. A. Marei, Bridging Markov chain Monte Carlo techniques and Tierney–Kadane approximations for progressively censored Garhy reliability models: simulation insights and a medical application, Mathematics, **14**, 1777 (2026).
[8] A. Algarni, A. M. Almarashi, F. Jamal, C. Chesneau and M. Elgarhy, Truncated inverse Lomax generated family of distributions with applications to biomedical data, J. Med. Imaging Health Inform., **11**, 2425–2439 (2021).
[9] A. S. Alghamdi et al., The sine alpha power-G family of distributions, Symmetry, **17**, 468 (2025).
[10] D. M. Ali, N. A. Noori and M. A. Khaleel, Characteristics and simulation of neutrosophic Gompertz-Burr-III distribution with real data application, AIP Conf. Proc., **3393**, 060008 (2026).
[11] I. Alkhairy, M. Nagy, A. H. Muse and E. Hussam, The Arctan-X family of distributions: properties, simulation, and applications to actuarial sciences, Complexity, **2021**, 4689010 (2021).
[12] T. W. Anderson and D. A. Darling, Asymptotic theory of certain goodness-of-fit criteria based on stochastic processes, Ann. Math. Stat., **23**, 193–212 (1952).
[13] L. J. Bain and M. Engelhardt, Statistical Analysis of Reliability and Life-Testing Models, Marcel Dekker, New York, (1991).
[14] Z. W. Birnbaum and S. C. Saunders, Estimation for a family of life distributions with applications to fatigue, J. Appl. Probab., **6**, 328–347 (1969).
[15] C. Chesneau and F. Jamal, The sine Kumaraswamy-G family of distributions, J. Math. Ext., 1–33 (2020).
[16] H. Cramér, On the composition of elementary errors, Scand. Actuar. J., **11**, 13–74 (1928).

© 2026 NSP
Natural Sciences Publishing Cor.

[17] S. Efromovich, Quasi-linear wavelet estimation, J. Amer. Statist. Assoc., **94**, 189–204 (1999).
[18] B. Elkalzah, M. O. Mohamed, K. Elsharkawy, E. S. Osman, A. Aldukeel and G. A. Marei, Classical and Bayesian estimation of stress-strength reliability under the discrete alpha-power Weibull distribution with incomplete and record data: application to high-voltage capacitors, AIMS Math., **11**, 6374–6399 (2026).
[19] E. Hussam, L. P. Sapkota and A. M. Gemeay, Tangent exponential-G family of distributions with applications in medical and engineering, Alex. Eng. J., **105**, 181–203 (2024).
[20] M. Imran, M. A. F. Elbarkawy, F. Jamal and G. A. Marei, An extended Lindley model with applications to entropy-based loss and actuarial risk measures, Comput. J. Math. Stat. Sci., **5**, 1–33 (2026).
[21] M. H. Jumaa, A. S. Qaddoori, S. A. Khalaf, N. A. Noori and M. A. Khaleel, Mathematical properties and simulations of the neutrosophic Gompertz-Inverse Burr-X distribution with application to under-five mortality, Iraqi J. Comput. Sci. Math., **6**, 23 (2025).
[22] J. H. K. Kao, Computer methods for estimating Weibull parameters in reliability studies, IRE Trans. Reliab. Qual. Control, **13**, 15–22 (1958).
[23] J. Lu, C. Liu, C. S. Yu and K. Wang, Determinants of accepting wireless mobile data services in China, Inf. Manag., **45**, 52–64 (2008).
[24] Z. Mahmood, C. Chesneau and M. H. Tahir, A new sine-G family of distributions: properties and applications, Bull. Comput. Appl. Math., 53–81 (2019).
[25] Z. Mahmood, T. M. Jawa, N. S. Ahmed, E. M. Khalil, A. H. Muse and A. H. Tolba, An extended cosine generalized family of distributions for reliability modeling: characteristics and applications with simulation study, Math. Probl. Eng., **2022**, 3634698 (2022).
[26] Z. Mahmood, T. M. Jawa, N. S. Ahmed, E. M. Khalil, A. H. Muse and A. H. Tolba, Sine π-power odd-G family of distributions with applications, Sci. Rep., **14**, 19481 (2024).
[27] A. J. Nawaf, M. H. Jumaa, N. A. Noori and M. A. Khaleel, Search and expand hybrid odd Lomax Fréchet distribution: properties, simulation, with application, in: UiTM International Conference on Mathematical Sciences, Springer Nature Singapore, 193–218 (2024).
[28] N. A. Noori and M. A. Khaleel, Development of the Gompertz-neutrosophic Lomax distribution: a four-parameter expansion for modeling uncertainty, AIP Conf. Proc., **3393**, 070084 (2026).
[29] K. A. Rashedi, L. S. Diab, A. H. Alenezy and G. A. Marei, A one-parameter decreasing-hazard lifetime model with exact inference on a bounded-below support, AIMS Math., **11**, 24445–24489 (2026).
[30] K. A. Rashedi, L. S. Diab, A. H. Alenezy and G. A. Marei, Inference for stress-strength reliability under unified hybrid censoring: a one-parameter model with applications, Mathematics, **14**, 2041 (2026).
[31] K. M. Sakthivel and J. Rajkumar, Transmuted sine-G family of distributions: theory and applications, Stat. Appl., 73–92 (2021).
[32] A. Schröter, T. Zimmermann and A. Zeller, Predicting component failures at design time, in: Proceedings of the 2006 ACM/IEEE International Symposium on Empirical Software Engineering, 18–27 (2006).
[33] A. S. Al-Moisheer, I. Elbatal, W. Almutiry and M. Elgarhy, Odd inverse power generalized Weibull generated family of distributions: Properties and applications, Math. Probl. Eng., **2021**, 5082192 (2021).
[34] S. Al-Marzouki, F. Jamal, C. Chesneau and M. Elgarhy, Topp-Leone odd Fréchet generated family of distributions with applications to COVID-19 data sets, Comput. Model. Eng. Sci., **125**, 437–458 (2020).
[35] S. A. Benchiha, L. P. Sapkota, A. Al Mutairi, V. Kumar, R. H. Khashab, A. M. Gemeay, M. Elgarhy and S. G. Nassr, A new sine family of generalized distributions: Statistical inference with applications, Math. Comput. Appl., **28**, 1–19 (2023).
[36] M. A. Aldahlan, F. Jamal, C. Chesneau, I. Elbatal and M. Elgarhy, Exponentiated power generalized Weibull power series family of distributions: Properties, estimation and applications, PLoS One, **15**, e0230004 (2020).
[37] A. S. Hassan and S. G. Nassr, Power Lindley-G family of distributions, Ann. Data Sci., **6**, 189–210 (2019).
[38] S. M. Alghamdi, M. Shrahili, A. S. Hassan, R. E. Mohamed, I. Elbatal and M. Elgarhy, Analysis of milk production and failure data: Using unit exponentiated half logistic power series class of distributions, Symmetry, **15**, 714 (2023).
[39] M. N. Atchadé, M. A. G. N'bouké, A. M. Djibril, A. Al Mutairi, M. S. A. Mustafa, E. Hussam, H. Alsuhabi and S. G. Nassr, A new Topp-Leone Kumaraswamy Marshall-Olkin generated family of distributions with applications, Heliyon, **10**, e24001 (2024).
[40] M. Elgarhy, E. I. Ali, S. Nasiru and A. W. Shawki, The complementary geometric Topp–Leone-G family of distributions with applications to insurance and engineering data, Eng. Rep., **7**, e70465 (2025).
[41] A. S. Hassan and S. G. Nassr, The inverse Weibull generator of distributions: Properties and applications, J. Data Sci., **16**, 723–742 (2018).
[42] M. Elgarhy, M. Nejib Ouertani, U. Abubakar, A. Ado Osi, H. Hamdani and M. Jobarteh, Arctangent Zubair-G family of distributions: Properties and applications to biomedical data, Eng. Rep., **7**, e70478 (2025).
[43] X. Tang, J.-T. Seong, R. Alharbi, A. Al Mutairi and S. G. Nassr, A new probabilistic model: Theory, simulation and applications to sports and failure times data, Heliyon, **10**, e25651 (2024).
[44] H. Haj Ahmad, E. M. Almetwally, M. Elgarhy and D. A. Ramadan, On unit exponential Pareto distribution for modeling the recovery rate of COVID-19, Processes, **11**, 232 (2023).
[45] M. Elgarhy, G. S. S. Abdalla, E. M. Almetwally, S. O. Bashiru, A. W. Shawki and A. M. Gemeay, Arctan inverted exponentiated Weibull model with actuarial measures and applications to insurance and inflation data, Sci. Afr., **2026**, e03260 (2026).
[46] Y. Shao and M. G. Hahn, Maximum product of spacings method: a unified formulation with illustration of strong consistency, Illinois J. Math., **43**, 489–499 (1999).

© 2026 NSP
Natural Sciences Publishing Cor.

[47] L. Souza, W. Junior, C. de Brito, C. Chesneau, T. Ferreira and L. Soares, On the Sin-G class of distributions: theory, model and application, J. Math. Model., 357–379 (2019).
[48] L. Souza, W. R. de Oliveira Júnior, C. C. R. de Brito, C. Chesneau, T. A. E. Ferreira and L. G. M. Soares, General properties for the Cos-G class of distributions with applications, Eurasian Bull. Math., 63–79 (2019).
[49] L. Souza, W. R. de Oliveira Júnior, C. C. R. de Brito, C. Chesneau, R. L. Fernandes and T. A. E. Ferreira, Tan-G class of trigonometric distributions and its applications, Cubo, 1–20 (2021).
[50] L. Souza, W. R. de Oliveira, C. C. R. de Brito, C. Chesneau, R. Fernandes and T. A. E. Ferreira, Sec-G class of distributions: properties and applications, Symmetry, **14**, 299 (2022).
[51] Q. Xia, Y. Tsong and Y. T. Weng, Methods and applications of percentile estimation, J. Biopharm. Stat., **30**, 267–276 (2020).

© 2026 NSP
Natural Sciences Publishing Cor.